Journal of Materials Chemistry A

Real-Time Observation of the Exchange Process between H2O and NO in the Metal-Organic Framework Ni-MOF-74

Journal:	*Journal of Materials Chemistry A*
Manuscript ID	TA-COM-09-2023-005265.R1
Article Type:	Communication
Date Submitted by the Author:	04-Jan-2024
Complete List of Authors:	Pandey, Haardik; Wake Forest University, Physics Wang, Hao; Rutgers University Alfaro, Monica ; University of North Texas, Department of Materials Science & Engineering Li, Jing; Rutgers The State University of New Jersey, Chemistry and Chemical Biology Thonhauser, Timo; Wake Forest University, Department of Physics Tan, Kui; University of North Texas System, Chemistry

COMMUNICATION

Real-Time Observation of the Exchange Process between H_2O and NO in the Metal-Organic Framework Ni-MOF-74

Received 00th January 20xx,
Accepted 00th January 20xx

DOI: 10.1039/x0xx00000x

Haardik Pandey,[a] Hao Wang,[b] Monica Vasquez Alfaro,[c] Jing Li,[b] Timo Thonhauser,[a]* Kui Tan[d]*

Molecular exchange is a common step occurring in many technological processes such as competitive adsorption, chemical separation, capture, delivery, and release. However, the underlying principle is not fully understood, especially in nanoconfined environments where the energetics and kinetics of such processes can deviate from that on flat surfaces. In this paper, we unravel the mechanism of a molecular exchange process by studying the displacement of NO by H_2O in Ni-MOF-74 in real-time using *in-situ* infrared spectroscopy combined with *ab initio* calculations. We show that weakly bound H_2O gradually displaces strongly bound NO on the metal sites by first weakening the M–N bond through forming H-bond and then moving the NO away so that it eventually desorbs. Interestingly, we further find that additional water facilitates this exchange by significantly lowering the kinetic barrier associated with this process as well as the overall energy of the final state. Although our study focuses on Ni-MOF-74, we believe that our finding and explanation of unexpected exchange phenomena—where strongly adsorbed molecules are apparently easily displaced by much weaker bound H_2O—is applicable to a much larger group of frameworks and will be helpful in designing and improving MOFs for real-world applications where humidity is often present.

Elucidating small molecule competitive adsorption behavior such as exchange processes in nanoporous materials is of great importance to both fundamental research and practical applications, including gas separation,[1-8] purification,[9-12] capture,[13-17] and molecule delivery and release.[18-20] Interest in using metal organic framework (MOF) materials for the purpose of absorbing molecules has grown enormously due to their extraordinary porosity, surface area, and structurally/chemically tunable functionality.[21, 22] Furthermore, their well-defined crystalline structure makes them a perfect platform to model molecular behavior in nanoconfined environments.[13, 23] Despite extensive studies conducted for single-component adsorption, explorations into the co-adsorption of multiple species—especially their dynamic competition—are still rather scarce due to the challenges in *in situ* characterization.[24-26] In such co-adsorption scenarios, two or more guest molecules competitively occupy the same adsorption sites, or one species displaces another pre-bound species from its primary binding site. In both processes, in general kinetic *and* thermodynamic factors are at play.[26] However, the nanoconfinement in MOFs provides a special environment which can cause unexpected effects due to additional intermolecular interactions or steric hinderances.

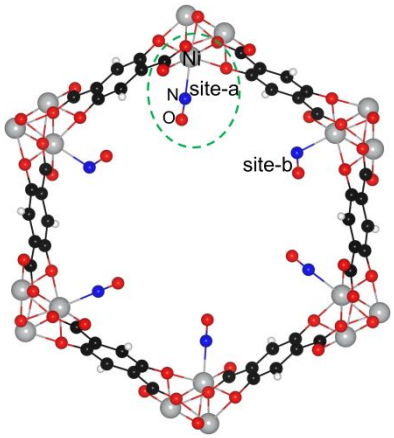

Figure 1. Ni-MOF-74-unit cell, shown here with NO molecules occupying all six available open-metal binding sites at the corners of the hexagonal channel.

In this work, we combine *in situ* infrared spectroscopy with *ab initio* calculations to investigate the exchange of H_2O with nitric oxide (NO) in the metal organic framework Ni-MOF-74. NO is an important biological signaling molecule.[27] Storage and safe delivery of NO based on the adsorbent material is promising for many antibacterial and antithrombotic applications.[28] The family of MOF-74 [M_2(dobdc), M = metal ions; dobdc = 2,5 dihydroxybenzenedicarboxylic acid]

[a] Department of Physics and Center for Functional Materials, Wake Forest University, Winston-Salem, NC 27109
[b] Department of Chemistry and Chemical Biology, Rutgers University, Piscataway, NJ 08854,
[c] Department of Materials Science & Engineering, University of Texas at Dallas, Richardson, Texas 75080
[d] Department of Chemistry, University of North Texas, Denton, TX 76203
* Corresponding author
Electronic Supplementary Information (ESI) available: [details of any supplementary information available should be included here]. See DOI: 10.1039/x0xx00000x

represents one of the best studied frameworks for single-component gas adsorption due to its well-characterized coordinatively unsaturated open-metal sites in its channel that serve as active binding sites for guest molecules, see Fig. 1. The specific binding affinity for different molecules depends highly on the exact guest-metal interaction. Notably, NO binds strongly with the open $Ni^{2+}$and Co^{2+} sites through the formation of nitrosyl species. The high binding affinity (~90 kJ/mol for Ni^{2+}, determined by calorimetry[29]) makes it impossible to be completely desorbed in dynamic vacuo and possible for efficient storage and delivery, but on the other hand, makes it possible to achieve efficient storage and delivery [27] It is observed that exposure of NO-loaded Ni-MOF-74 to water moisture results in gradual removal of NO.[27, 29] This is very surprising in that single-component H_2O studies find the water binding enthalpy in Ni-MOF-74 at ~ 60 kJ/mol,[30] significantly less than that of NO. This prompted us to carry out a detailed examination of the energetics and kinetics of the $H_2O \rightarrow NO$ exchange process in Ni-MOF-74. Surprisingly, our results show that the thermodynamics of H_2O + NO co-adsorption differs noticeably from their single-component adsorption. Specifically, in the mixture it is energetically more favorable for H_2O to occupy the metal centers even though its binding energy is weaker than that of NO. We further show how H_2O displaces preabsorbed NO through synergistic interactions of multiple molecules that significantly reduce the kinetic barrier for this process. Remarkably, the detailed steps of the exchange process can be directly observed and probed with IR spectroscopy in real-time, which shows clear evidence that addition of water first weakens the Ni–NO bond and then displaces NO from the metal sites.

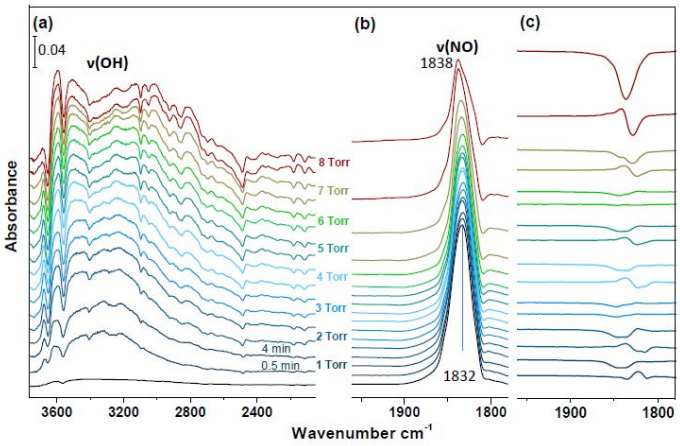

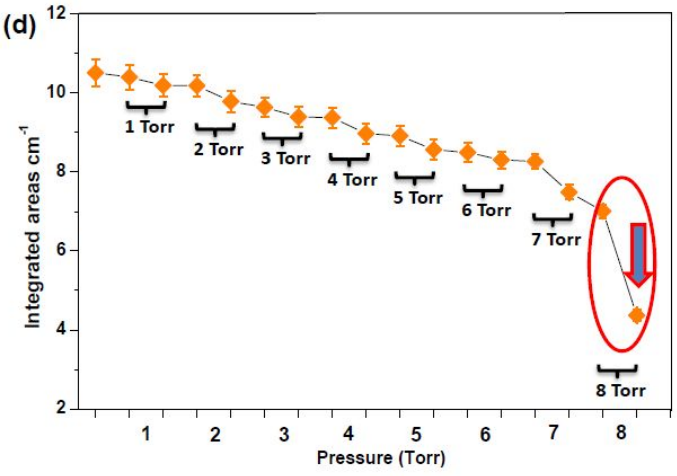

Figure 2. (a/b) IR spectra of loading H_2O into Ni-MOF-74 with pre-adsorbed NO as a function of vapor pressure showing the stretching (ν) bands of adsorbed H_2O and NO, respectively. At each pressure point, the vapor was kept inside the cell for ~4 min. The spectra were recorded at the beginning (~0.5 min) and end (~4 min) of H_2O exposure. All spectra are referenced to the activated MOF in vacuum (<20 mTorr). **(c)** Differential spectra, obtained by referencing each spectrum to the previous data, showing the perturbation and decrease of the pre-adsorbed NO band upon loading H_2O vapor. **(d)** Evolution of integrated areas of the ν(NO) band upon loading H_2O as a function of pressure. Each pressure contains the points at the beginning (~0.5 min) and end (~4 min) of the loading process.

The experiment was started by loading NO alone into Ni-MOF-74 at 40 Torr for 10 min, which is sufficient for NO adsorption to reach uptake saturation yet without destroying crystalline MOF structure (see Fig. S3). The binding of NO onto open Ni^{2+} sites is characterized by observing a ν(NO) band at 1832 cm^{-1},[29, 31] which downward (red) shifts by 44 cm^{-1} with respect to the gas-phase value at 1876 cm^{-1}. Such a shift is caused by the well-known π back-donation effect from the metal into antibonding orbitals of nitrosyl species, thus weakening the N–O bond.[32] The strong binding of $Ni^{2+}\cdots$NO leads to the large hysteretic effect in NO desorption shown in Fig. S4, i.e., the intensity of the ν(NO) band decreased by less than 10% after 30 min of evacuation at 25 °C. This slow desorption rate allows us to investigate the effect of H_2O exposure on the metal-bound NO species. For the NO + H_2O co-adsorption study, we first loaded pure NO inside Ni-MOF-74 at 40 Torr. After the adsorption reached saturation, the sample was evacuated for ~3 min until the pressure drops below 20 mTorr. Then H_2O vapor was introduced as a function of pressure from ~1 Torr to ~8 Torr. The intensity of the ν(NO) band was measured during the water exposure. Fig. 2 shows a continuous decrease of the ν(NO) band along with an increase of the broad ν(OH) band upon loading H_2O vapor, indicating that pre-adsorbed NO on the Ni^{2+} sites was gradually displaced by incoming H_2O and eventually exited the MOF channels. Notably, above ~7 Torr, a steep drop of the ν(NO) band was observed, corresponding to a significant loss of metal-bound NO; the ν(NO) band shifts to a higher frequency at 1838 cm^{-1}; the center of the intense ν(OH) band gradually shifts to a lower frequency around 3180 cm^{-1}, indicating the formation of hydrogen-bonded water clusters.[33, 34] Careful examination of the ν(NO) band evolution (see Fig. 2b) reveals that at each pressure point the ν(NO) band does not immediately diminish upon contact with more water vapor. Instead, it takes a certain amount of time (~4 min) to decrease. This indicates that there is a slow exchange kinetics between H_2O and NO. To reveal more mechanistic insight, we plotted the differential spectra in Fig. 2c, showing the detailed H_2O–NO exchange process. Interestingly, we found that, upon adding water vapor, the ν(NO) band first slightly shifts back to higher frequency (indicated by the derivative-like feature) and then decreases in intensity (shown by the loss of the ν(NO) band centered at this higher frequency position). The upward (blue-) shift gives an indication of reduced π-back-bonding between Ni^{2+} and NO, and the intensity decrease implies the removal of NO from the Ni^{2+} site. This indicates that incoming water first weakens the M–N bond and then displaces NO from the Ni^{2+} site. We have then checked the $H_2O \rightarrow NO$ exchange process in isostructural Co-MOF-74 materials that also exhibit strong binding toward NO through formation of nitrosyl species. The observation is quite similar to Ni-MOF-74 in that loading H_2O first results in a blue shift of the ν(NO) band, corresponding to the weakening of the Co-N bond, and eventually displaces cobalt-bound NO above 7 Torr (see Fig. S5). However, our observations in Co-MOF-74 are different from Ti-MOF-74: in Ti-MOF-74 a redox

reaction of NO with the OH-terminating groups leads to the formation of strong covalent Ti–NO bonds that are resistant to water insertion.[35]

To further understand this unexpected exchange process, we employed *ab initio* calculations to help us interpret our IR spectra and analyze the interactions between NO and H_2O inside Ni-MOF-74 channels. The Ni-MOF-74 unit cell used for our calculations consists of six Ni atoms and was optimized to its energy minimum. Binding trends of NO and H_2O molecules were then studied at different sites, showing that NO has the higher binding energy of 71 kJ/mol at the Ni site, as compared to 66 kJ/mol for H_2O. Based on these single-component binding energies, one would predict that the exchange of NO by H_2O is energetically unfavorable. This, however, seems to contradict our IR measurements in Fig. 2, which show that H_2O can displace NO from the open metal position, and this replacement becomes easier as water loading increases. We begin our analysis of the NO/H_2O interaction by performing calculations on a Ni-MOF-74 unit cell pre-loaded with 6 NO atoms, occupying all the open metal sites (see Fig. 1). Then, we introduced one, two and, three H_2O guest molecules in order to study the NO–H_2O interaction at varying H_2O concentrations. We focus our calculations on one of the Ni^{2+} sites (site-a in Fig. 1). Figure 3 shows the relaxed initial structures (formed on addition of H_2O) and final structures (after H_2O replaces NO) used to study the one, two, and three H_2O cases. The first H_2O, when placed close to the Ni, binds to the nearest O atom (Fig. 3b1). The induced charge densities for all three cases of H_2O adsorption in Fig. 3b1, 3c1, and 3d1 show strong H-bonding interactions between the water and O of the ligand.

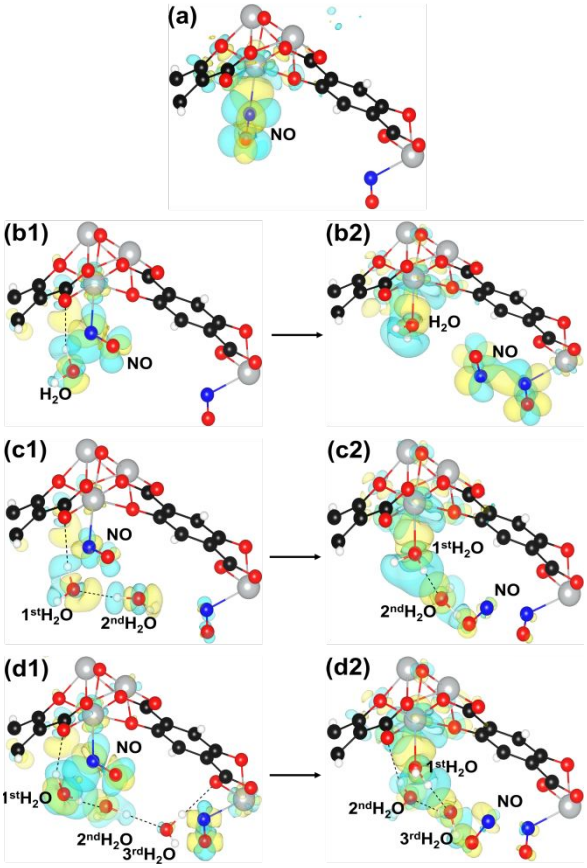

Figure 3. Molecular configurations and induced charge densities (i.e., charge density rearrangements as a result of the bond formation) at the primary binding site for **(a)** NO bound to Ni, and for initial/final structures of the $H_2O \rightarrow$ NO exchange for the cases of **(b1/b2)** one H_2O, **(c1/c2)** two H_2O, and **(d1/d2)** three H_2O. Yellow areas show charge accumulation and blue ones show charge depletion; iso-levels are set to 0.001 e/Å^3.

Transition-state searches were carried out to better understand the energetics involved in the above mentioned one, two, and three H_2O+MOF cases. Figures 3b1, 3c1, and 3d1 were taken as the starting configurations for studying the exchange of NO by H_2O, using the climbing-image nudged elastic band (cNEB) formalism.[36, 37] The final images (Figs. 3b2, 3c2, 3d2 and Fig. S6) were formed by replacing NO with the attacking H_2O (1^{st} H_2O bonded to the O atom) and then relaxing the resulting configurations to their energy minima. Results are shown in Fig. 4. For only one H_2O molecule present at the metal site (Fig. 3b1), the exchange is energetically slightly favorable, even though in single-component studies NO binds more strongly. The reason for this is that, in the initial structure, the H_2O bound at the oxygen ligand shows a binding energy of 30 kJ/mol and, in the final configuration, the displaced NO is now interacting with the NO at the neighboring site-b with a binding energy of 37 kJ/mol. This adds up to a comparable contribution to the total energies of the initial and final structures. An important aspect is observed when comparing the induced charge densities before (Fig. 3a) and after addition of H_2O (Fig. 3b1). We can observe that the charge accumulation (yellow lobe) at the NO–Ni bond has shifted to a depletion of charge (blue lobes), thus pointing to a weaking of the NO–Ni bond upon the introduction of one H_2O as evidenced by a blue shift of the ν(NO) band in the differential spectra of Fig. 2b. The kinetic barrier for the $H_2O \rightarrow$ NO exchange process is rather high (46.7 kJ/mol, red line in Fig. 4) and accounts for the observation of slow kinetics for the $H_2O \rightarrow$ NO exchange at low vapor pressures in our IR measurements.

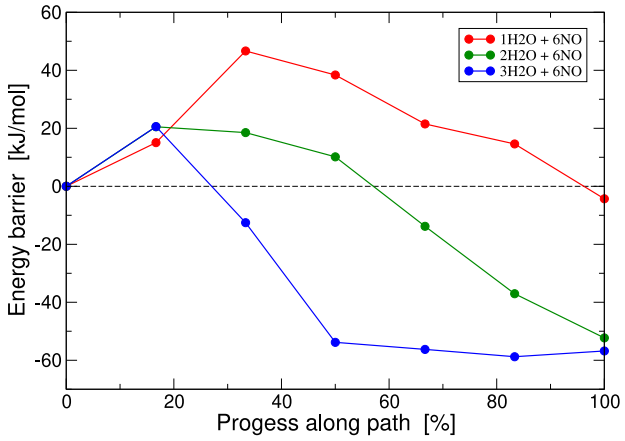

Figure 4. Transition-state searches showing the minimum energy path for H_2O replacing NO from the metal center.

The introduction of a second H_2O to site-a results in a considerable lowering of the energy barrier to 20.6 kJ/mol (green line in Fig. 4). Surprisingly, the post-exchange structure has a much-lowered total energy relative to the starting configuration. The energetics for this case can be analyzed by first looking at the binding energy for the second H_2O that shows a binding of 32 kJ/mol in the initial structure but increases to 54 kJ/mol in the final structure, as it is able to interact better with the first H_2O that is now occupying the preferable metal binding site. This can be seen in Fig. 3c2, which shows a greater change in the charge densities from the previous configuration in Fig. 3c1. When comparing Fig. 3b1 and 3c1, we also clearly see that the presence of a second H_2O molecule even further reduces the amount of charge accumulation in the Ni–NO bond as represented by a large reduction of the yellow-colored area at the

NO–Ni bond. This shows that the presence of a second H_2O—which increases the H_2O concentration in the unit cell—negatively affects the bond at the Ni^{2+} metal site, as evidenced by the slight blue-shift of the ν(NO) band observed in the differential spectra in Fig. 2c. This makes the replacement of NO by H_2O more favorable in the presence of a second H_2O molecule at the metal site and explains the very low energy barrier in our transition-state results. This is also in agreement with our IR results, which show that—as the H_2O vapor pressure reaches a particular threshold (~7 Torr) and H-bonded water clusters form—a sudden reduction of Ni^{2+}-bound NO takes place. When the concentration of H_2O is further increased by adding a third H_2O at site-a, we see in Fig. 3d1 that the third H_2O does not bind on site-a and instead moves to the O atom at site-b. Thus, the corresponding transition-state results are similar to the case of two H_2O, with the same energy barrier of 20.6 kJ/mol and a similar relative total energy of the final configuration. The energetical favorability is further confirmed by measuring H_2O and NO during their simultaneous introduction into the sample (see Fig. S7), which shows that H_2O preferentially adsorbs within Ni-MOF-74 and hinders NO occupation of the metal sites.

In summary, we combined *in situ* IR spectroscopy and *ab initio* calculations to reveal the detailed exchange process of H_2O and NO in Ni-MOF-74 and uncover its energetics and kinetics. We show that it is more energetically favorable for H_2O to occupy the open-metal sites than NO, especially at high water loading, despite the stronger binding energy of NO in single-component studies. Notably, we have identified experimentally and computationally that water first adsorbs at the nearby phonate site and weakens the metal–N bond of the nitrosyl species through H-bonding interactions, and then displaces it from the metal sites. The former is an important precursor for the exchange process that follows. Loading extra H_2O can further decrease the metal–N bond strength and make the process readily occur by lowering its kinetic barrier. These findings shed important light onto molecular exchange processes in nanoporous materials and show that single-component adsorption studies may not be suitable to predict the behavior of the more complex multi-component co-adsorption of gas mixtures.

Conflicts of interest

There are no conflicts to declare.

Acknowledgements

This work was entirely supported by the U.S. Department of Energy, Office of Science, Office of Basic Energy Sciences under award DE-SC0019902.

Notes and references

1. J.-R. Li, J. Sculley and H.-C. Zhou, *Chemical Reviews*, 2011, **112**, 869-932.
2. R.-B. Lin, S. Xiang, W. Zhou and B. Chen, *Chem*, 2020, **6**, 337-363.
3. X. Zhao, Y. Wang, D.-S. Li, X. Bu and P. Feng, *Advanced Materials*, 2018, **30**, 1705189.
4. E. D. Bloch, W. L. Queen, R. Krishna, J. M. Zadrozny, C. M. Brown and J. R. Long, *Science*, 2012, **335**, 1606-1610.
5. K.-J. Chen, D. G. Madden, S. Mukherjee, T. Pham, K. A. Forrest, A. Kumar, B. Space, J. Kong, Q.-Y. Zhang and M. J. Zaworotko, *Science*, 2019, **366**, 241.
6. A. Cadiau, K. Adil, P. M. Bhatt, Y. Belmabkhout and M. Eddaoudi, *Science*, 2016, **353**, 137-140.
7. L. Li, R.-B. Lin, R. Krishna, H. Li, S. Xiang, H. Wu, J. Li, W. Zhou and B. Chen, *Science*, 2018, **362**, 443.
8. D. Banerjee, A. J. Cairns, J. Liu, R. K. Motkuri, S. K. Nune, C. A. Fernandez, R. Krishna, D. M. Strachan and P. K. Thallapally, *Accounts of Chemical Research*, 2015, **48**, 211-219.
9. R. Sahoo and M. C. Das, *Coordination Chemistry Reviews*, 2021, **442**, 213998.
10. D. Britt, H. Furukawa, B. Wang, T. G. Glover and O. M. Yaghi, *Proceedings of the National Academy of Sciences*, 2009, **106**, 20637-20640.
11. R.-B. Lin, S. Xiang, H. Xing, W. Zhou and B. Chen, *Coordination Chemistry Reviews*, 2019, **378**, 87-103.
12. J. B. DeCoste and G. W. Peterson, *Chemical Reviews*, 2014, **114**, 5695-5727.
13. T. M. McDonald, J. A. Mason, X. Kong, E. D. Bloch, D. Gygi, A. Dani, V. Crocellà, F. Giordanino, S. O. Odoh, W. S. Drisdell, B. Vlaisavljevich, A. L. Dzubak, R. Poloni, S. K. Schnell, N. Planas, K. Lee, T. Pascal, L. F. Wan, D. Prendergast, J. B. Neaton, B. Smit, J. B. Kortright, L. Gagliardi, S. Bordiga, J. A. Reimer and J. R. Long, *Nature*, 2015, **519**, 303-308.
14. J.-B. Lin, T. T. Nguyen Tai, R. Vaidhyanathan, J. Burner, M. Taylor Jared, H. Durekova, F. Akhtar, K. Mah Roger, O. Ghaffari-Nik, S. Marx, N. Fylstra, S. Iremonger Simon, W. Dawson Karl, P. Sarkar, P. Hovington, A. Rajendran, K. Woo Tom and K. H. Shimizu George, *Science*, 2021, **374**, 1464-1469.
15. K. Sumida, D. L. Rogow, J. A. Mason, T. M. McDonald, E. D. Bloch, Z. R. Herm, T.-H. Bae and J. R. Long, *Chemical Reviews*, 2011, **112**, 724-781.
16. P. Nugent, Y. Belmabkhout, S. D. Burd, A. J. Cairns, R. Luebke, K. Forrest, T. Pham, S. Ma, B. Space, L. Wojtas, M. Eddaoudi and M. J. Zaworotko, *Nature*, 2013, **495**, 80-84.
17. J. E. Mondloch, M. J. Katz, W. C. Isley Iii, P. Ghosh, P. Liao, W. Bury, G. W. Wagner, M. G. Hall, J. B. DeCoste, G. W. Peterson, R. Q. Snurr, C. J. Cramer, J. T. Hupp and O. K. Farha, *Nature Materials*, 2015, **14**, 512-516.
18. M.-X. Wu and Y.-W. Yang, *Advanced Materials*, 2017, **29**, 1606134.
19. P. Horcajada, T. Chalati, C. Serre, B. Gillet, C. Sebrie, T. Baati, J. F. Eubank, D. Heurtaux, P. Clayette, C. Kreuz, J.-S. Chang, Y. K. Hwang, V. Marsaud, P.-N. Bories, L. Cynober, S. Gil, G. Ferey, P. Couvreur and R. Gref, *Nature Materials*, 2010, **9**, 172-178.
20. J. D. Della Rocca, D. Liu and W. Lin, *Acc. Chem. Res.*, 2011, **44**, 957.
21. H. Furukawa, K. E. Cordova, M. O'Keeffe and O. M. Yaghi, *Science*, 2013, **341**, 1230444.
22. H. C. Zhou, J. R. Long and O. M. Yaghi, *Chem. Rev.*, 2012, **112**, 673.
23. S. Krause, V. Bon, I. Senkovska, U. Stoeck, D. Wallacher, D. M. Többens, S. Zander, R. S. Pillai, G. Maurin, F. X. Coudert and S. Kaskel, *Nature*, 2016, **532**, 348.
24. W. You, Y. Liu, J. D. Howe and D. S. Sholl, *The Journal of Physical Chemistry C*, 2018, **122**, 8960-8966.

25. L. Hamon, P. L. Llewellyn, T. Devic, A. Ghoufi, G. Clet, V. Guillerm, G. D. Pirngruber, G. Maurin, C. Serre, G. Driver, W. van Beek, E. Jolimaître, A. Vimont, M. Daturi and G. Férey, *Journal of the American Chemical Society*, 2009, **131**, 17490-17499.
26. K. Tan, S. Zuluaga, Q. Gong, Y. Gao, N. Nijem, J. Li, T. Thonhauser and Y. J. Chabal, *Chemistry of Materials*, 2015, **27**, 2203-2217.
27. A. C. McKinlay, B. Xiao, D. S. Wragg, P. S. Wheatley, I. L. Megson and R. E. Morris, *Journal of the American Chemical Society*, 2008, **130**, 10440-10444.
28. S. Keskin and S. Kızılel, *Industrial & Engineering Chemistry Research*, 2011, **50**, 1799-1812.
29. F. Bonino, S. Chavan, J. G. Vitillo, E. Groppo, G. Agostini, C. Lamberti, P. D. C. Dietzel, C. Prestipino and S. Bordiga, *Chemistry of Materials*, 2008, **20**, 4957-4968.
30. P. Canepa, C. A. Arter, E. M. Conwill, D. H. Johnson, B. A. Shoemaker, K. Z. Soliman and T. Thonhauser, *Journal of Materials Chemistry A*, 2013, **1**, 13597-13604.
31. B. Barth, M. Mendt, A. Pöppl and M. Hartmann, *Microporous and Mesoporous Materials*, 2015, **216**, 97-110.
32. C. Lamberti, A. Zecchina, E. Groppo and S. Bordiga, *Chemical Society Reviews*, 2010, **39**, 4951-5001.
33. O. Byl, J.-C. Liu, Y. Wang, W.-L. Yim, J. K. Johnson and J. T. Yates, *Journal of the American Chemical Society*, 2006, **128**, 12090-12097.
34. K. Tan, S. Zuluaga, Q. Gong, P. Canepa, H. Wang, J. Li, Y. J. Chabal and T. Thonhauser, *Chemistry of Materials*, 2014, **26**, 6886-6895.
35. S. Jensen, K. Tan, L. Feng, J. Li, H.-C. Zhou and T. Thonhauser, *Journal of the American Chemical Society*, 2020, **142**, 16562-16568.
36. G. Henkelman, B. P. Uberuaga and H. Jonsson, *The Journal of Chemical Physics*, 2000, **113**, 9901-9904.
37. G. Henkelman and H. Jónsson, *The Journal of Chemical Physics*, 2000, **113**, 9978-9985.